iScience

CellPress
OPEN ACCESS

Article

Broadband acoustic illusion coating based on thin conformal metasurface

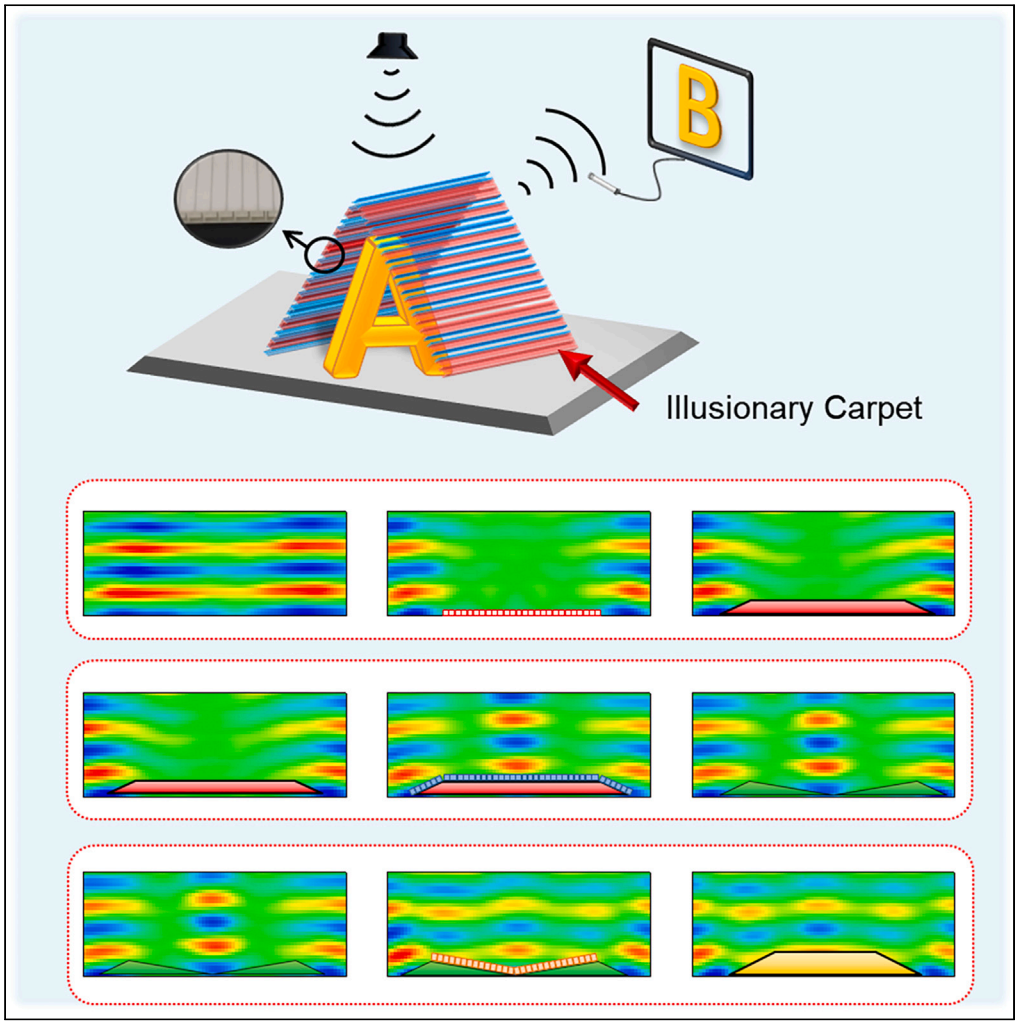

Kangyao Sun, Fuli Zhang, Shuang Chen, Quanhong Fu, Yali Zeng, Yuancheng Fan

fuli.zhang@nwpu.edu.cn (F.Z.)
phyfan@nwpu.edu.cn (Y.F.)

Highlights

Two types of metacells are designed to steer phase from 0 to 2π in a broadband

Illusion coating is proposed for reshaping the scattering fields

The illusion broadband performance up to 40.5%

Sun et al., iScience 27, 110504
August 16, 2024
https://doi.org/10.1016/j.isci.2024.110504

iScience

CellPress
OPEN ACCESS

Article

Broadband acoustic illusion coating based on thin conformal metasurface

Kangyao Sun,[1] Fuli Zhang,[1,3,*] Shuang Chen,[2] Quanhong Fu,[1] Yali Zeng,[1] and Yuancheng Fan[1,*]

SUMMARY

Acoustic metasurface with rationally distributed phase manipulating characteristic provides a promising platform to reshape the wavefront of scattering wave. Such acoustic illusion carpet suffers from limitation of narrow bandwidth and relatively large volume to contain the object to be hidden. Here, we propose and experimentally demonstrate broadband conformal acoustic illusion coatings composed of subwavelength-thick metacells that are designed by two types of modified Helmholtz resonators with 2π reflection phase. By deliberate design of reflection phase distributions of illusion coating, the reflected wavefront can be reshaped between trapezoid and triangles and vice versa. Furthermore, an enlarged illusion is obtained by this methodology. More importantly, the illusion behaviors are verified both numerically and experimentally from 3000 Hz to 4500 Hz, resulting in relatively broad bandwidth up to 40.5%, which is definitely of extreme importance for potential applications.

INTRODUCTION

Over the past few years, artificial composite materials for controlling the flow of acoustic wave such as metamaterials, have attracted more and more attention for their arbitrarily designed constitutive properties. Acoustic metamaterials with reconfigurable structures have been developed to achieve many unusual and exciting acoustic characteristics based on local resonance, such as negative mass density, bulk modulus, and refractive index.[1–5] The novel characteristics make acoustic metamaterials promising on effectively engineering the transmission behavior of acoustic waves in subwavelength scale,[6–13] particularly the manipulation of acoustic wavefront in military applications, such as acoustic invisible cloak.[14,15] Acoustic invisible cloak is proposed to hide an object by guiding the acoustic wavefronts around the hidden object without any distortion,[16] due to its excellent capability of manipulating the acoustic propagation characteristics in the bulk of it.

Comparing with acoustic metamaterial, a two-dimensional metasurface is designed for controlling the acoustic scattering properties on the surface of it. Acoustic metasurface with deep-subwavelength thickness and simpler geometry can also be employed for steering acoustic waves effectively.[17–22] Tremendous researches have focused on metasurfaces for practical applications in e.g., low-frequency noise control,[23,24] and wavefront manipulation[25–31] of acoustic waves in small scales. With proper design of metasurfaces, various interesting applications have been realized such as perfect absorber,[32] superlens,[33,34] and orbital angular momentum.[35] In addition, acoustic metasurface also provides a feasible platform for the design of light invisible cloak by offering phase shifts to compensate the phase distortion introduced by the detected target.[36–40]

As the generalization of the cloak, illusion carpet is proposed as a new scheme to achieve more luxuriant manipulation of wave based on transformation optics.[41] However, the optical illusion device based on transformation optics is difficult to realize because it is composed of bulky distributed metamaterials with simultaneously negative permittivity and permeability. As the counterpart of the optical cloak[42] and illusion,[43,44] acoustic illusion has also been studied intensively.[45–50] With introduction of the illusion device, the detector will be cheated and mistake the illusion for the true object. Therefore, acoustic illusion carpet is an advanced artificial structure that not only hides the detected target, but also replaces the target with an illusion. However, the illusion performance based on transformation acoustics is designed with complex theories. As a result, acoustic illusion carpet based on generalized Snell's law is considered to generate an illusion before the target.[48,49] Owing to the excellent phase manipulation capability and simple structural design,[51–55] metasurface is a promising candidate that renders a simpler way to realize the illusion performance.

In this paper, we demonstrate illusion coatings for realizing various manipulations on the scattering fields of acoustic target in a broadband. The designed illusion coating is made of two types of modified Helmholtz resonators which are rationally designed for full-range (i.e., 2π) phase modulation and controlled dispersion characteristic for broadband response. By delicately designing the resonator array as well as the phase gradient distribution based on generalized Snell's law, the illusion coating can compensate the local phase of scattering field for mimicking the scattering field of desired object. Due to the coatings are attached on the surface of the acoustic object, the designed

[1]MOE Key Laboratory of Material Physics and Chemistry Under Extraordinary Conditions, School of Physical Science and Technology, Northwestern Polytechnical University, Xi'an 710129, China
[2]Shaanxi Huayan Aero-instrument Co. Ltd, Xi'an 710129, China
[3]Lead contact
*Correspondence: fuli.zhang@nwpu.edu.cn (F.Z.), phyfan@nwpu.edu.cn (Y.F.)
https://doi.org/10.1016/j.isci.2024.110504

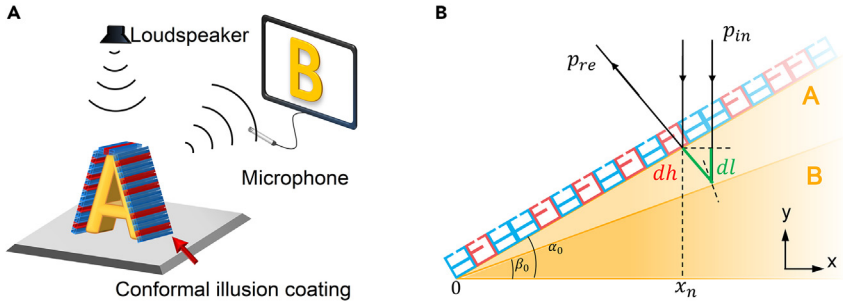

Figure 1. Schematic of a 2D illusion coating

(A) The conformal illusion coating can shift the scattering field of object A to object B with a totally different profile from object A.

(B) The operation principle of the metacells. The phase shift of the *n*th metacell is in proportion to dl (the green lines) which is determined by the height difference dh between object A and object B.

conformal metasurface requires less space than the traditional illusion carpet. The illusion performances are realized in a broadband for objects with one trapezoid, two triangles and an enlarged geometry. The broadband response is due to that the metacells of the illusion coating are designed with continuously varying phase modulation without any resonance in the operation band. The illusion performances are experimentally verified under the detection of a 2D scanning stage for air-borne acoustic wave propagation from 3000 Hz to 4500 Hz with a bandwidth of 40.5%. The demonstrated illusion coating is promising for freely manipulating the scattering field of more complex acoustic targets.

RESULTS

Methodology of conformal illusion coating

The proposed illusion coating is made of an array of ultrathin metacells containing two kinds of modified Helmholtz resonators (see Figure 1A, depicted by red and blue structures) for manipulating the acoustic scattering. Object A is an acoustic target for being detected. Considering an acoustic plane wave traveling normally on the surface of object A, the scattering field will be detected by a microphone and exhibited on a screen. When we cover a conformal acoustic illusion coating by attaching metacells on the surface of object A, the phase gradient distribution of the scattered acoustic wave of object A can be reshaped, forming the same scattering field as an object B by the metacells with properly designed structural parameters. It indicates that with introduction of a conformal illusion coating, the detector is cheated and it cannot achieve the true scattering field of the detected target. Meanwhile, the added bulk of the detected target is negligible.

The operation principle of the metacells is shown in Figure 1B. To illustrate the strategy of the illusion coating, we consider two triangular object A and B with base angles α_0 and β_0, as shown in Figure 1B. Object A is covered with an illusion coating for being reshaped to object B. We suppose that the *x*-coordinate of the *n*th metacell on the ground is x_n. In this case, x_n is expressed as

$$x_n = \frac{(2n-1)\cdot l\cdot\cos(\alpha_0)}{2} \quad \text{(Equation 1)}$$

The height difference dh between A and B at x_n is given as

$$dh = x_n\cdot(\tan\alpha_0 - \tan\beta_0) \quad \text{(Equation 2)}$$

The phase difference $d\varphi$ caused by the acoustic distance dl at x_n can be achieved as[19]

$$d\varphi = -k_0\cdot dl \quad \text{(Equation 3)}$$

where $k_0 = 2\pi f_0/c_0$ is the wave vector at f_0, $c_0 = 343$ m/s is the sound speed in air and $dl = 2dh\cdot\cos^2\beta_0$.

Therefore, in order to compensate the phase difference, the added phase caused by the *n*th metasurface cell should be $-d\varphi$.

Design of acoustic resonators with full-range phase response

The designed 2D metasurface is made of two kinds of metacells, as shown in Figure 2A. Each metacell consists of a cavity with a plate in it and a slit on the upper surface. The profiles of Cell A and Cell B are uniform (with height $h = 12$ mm, length $l = 10$ mm, width of slit $s = 1$ mm, thickness of upper and lower surfaces $t = 1$ mm and wall is $t/2$). Identical longitudinal and transversal dimensions of the metacells are advantageous in the modulation of the scattered wave. Length of plates in the cavities is $l_A = 8$ mm or $l_B = 9$ mm respectively. Cell A with an inner plate can be regarded as two series cavities, and sum of the height of the two cavities is a constant. For Cell B, the inner plate cut the metacell into two parts: an upper cavity and a lower space. It can be seen that only the upper cavity can manipulate the acoustic wave efficiently. By tuning the distance d between the plate and the upper surface, the impedance characteristics of Cell A or Cell B will be changed and the local phase of scattering field will be modulated accordingly. The modulation performance of the proposed metacells on the scattered wave is achieved by simulation, as shown in Figure 2B. In the frequency range from 2000 Hz to 5000 Hz, the phase shifts induced by the metacells vary almost from 0 to 2π with d varying from 0.01 mm to 9.99 mm. It indicates that the metacells with the varying parameter d can modulate

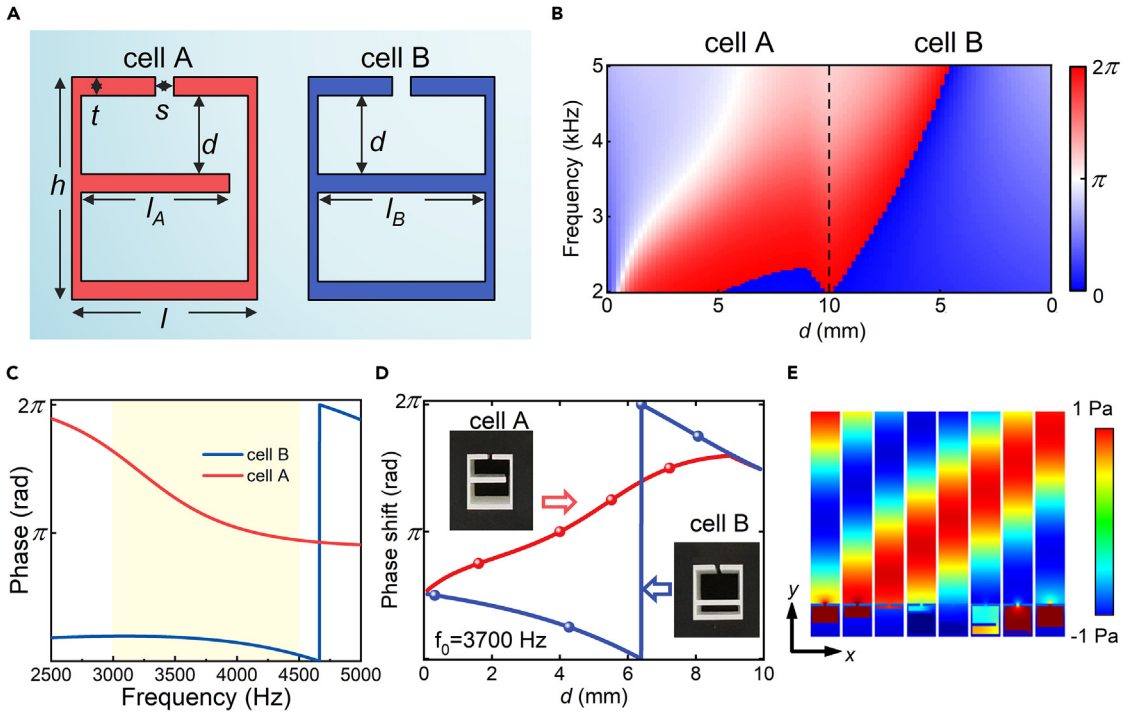

Figure 2. Phase modulation characteristics of metacells

(A) Illustration of the proposed two metacells Cell A (red structure) and Cell B (blue structure), which are capable of properly modulating the local phase of scattering field with full-range (i.e., 2π).

(B) The phase response induced by Cell A (left part of the dotted line) and Cell B (right part) in the frequency range from 2000 Hz to 5000 Hz.

(C) The phase response induced by Cell A (red curve) and Cell B (blue curve) as a function of frequency *f*, at *d* = 5 mm.

(D) The phase response induced by Cell A (red curve) and Cell B (blue curve) as a function of structural parameter *d*, at f_0 = 3700 Hz. The eight dots refer to the phases from 0 to 2π with a step of π/4. The inserts are photos of designed metacells made by 3D-printing technology.

(E) Simulated scattering fields of individual metacells corresponding to the eight dots shown in (D) at f_0.

the wavefront of acoustic waves effectively in a wide frequency range. Moreover, the phase shifts induced by the metacells vary continuously without any resonance in Figure 2B that means the metacells working away from the resonant frequency in the simulated frequency range.

Here, we focus our studies on 3700 Hz where the curves of the phase shifts are nearly linear. It means that the phase shift changes uniformly with the variation of *d* at the certain frequency. The relationship between the phase shift and the parameter *d* achieved in simulation is shown in Figure 2D. By changing *d* with a step 0.01 mm, the phase shifts in Cell A are adjusted from 1.69 rad to 4.69 rad, and the phase shifts in Cell B are adjusted from 0 to 1.60 rad and 4.69 rad–6.28 rad. It is exciting to find that, the phase shifts, caused by Cell A and Cell B, changed almost the full 2π range. Hence we can shift the wavefront of scattered wave freely by choosing the parameters *d* of metacells with delicate calculation. The ratio between the thickness of sample (12.0 mm) and the wavelength studied in the experiment (92.8 mm) is about 0.129. Therefore, the scale of the metasurfaces is in a sub-wavelength region. Besides, it is still worthwhile to point out that, by choosing suitable size of the metacells, approximate linear phase shifts can be achieved at any frequency from 2000 Hz to 5000 Hz, as shown in Figure 2B. Figure 2C illustrates the phase response induced by Cell A (red curve) and Cell B (blue curve) as a function of frequency *f*, at *d* = 5 mm, for a more visual representation. In the range of 3000–4500 Hz, the phase changes almost linearly as the frequency increases. The eight dots in Figure 2D refer to the phase shifts from 0 to 2π with a step of π/4. The energy loss of the metacells is also studied in thermosviscous acoustic field. As Figure 2E shows, the scattering fields correspond to the eight dots in Figure 2D when the acoustic pressure of incident wave is 1 Pa. It can be seen that all the amplitudes of the scattered waves approach to 1 Pa, which means there are few thermal and viscous effects in the metacells so we can leave out the energy loss for the rest of the simulation.

Validation of conformal illusion coating

Based on the excellent phase modulation characteristics of the proposed metacells, we introduce the idea of illusion coatings for mimicking the scattering field of desired object. Three illusion coatings are designed, respectively, to create an illusion the same as a trapezoid out of thin air by coating I, cut the trapezoid into two triangles under the total cover of coating II and reshape the two triangles to an enlarged trapezoid under partial cover of coating III. Both simulated and measured illusion performances are demonstrated to verify that the properly designed illusion coatings are capable of compensating the local phase of two different objects for achieving the same scattering fields. In our study, numerical simulations are performed by using the finite-element software COMSOL Multiphysics. In the

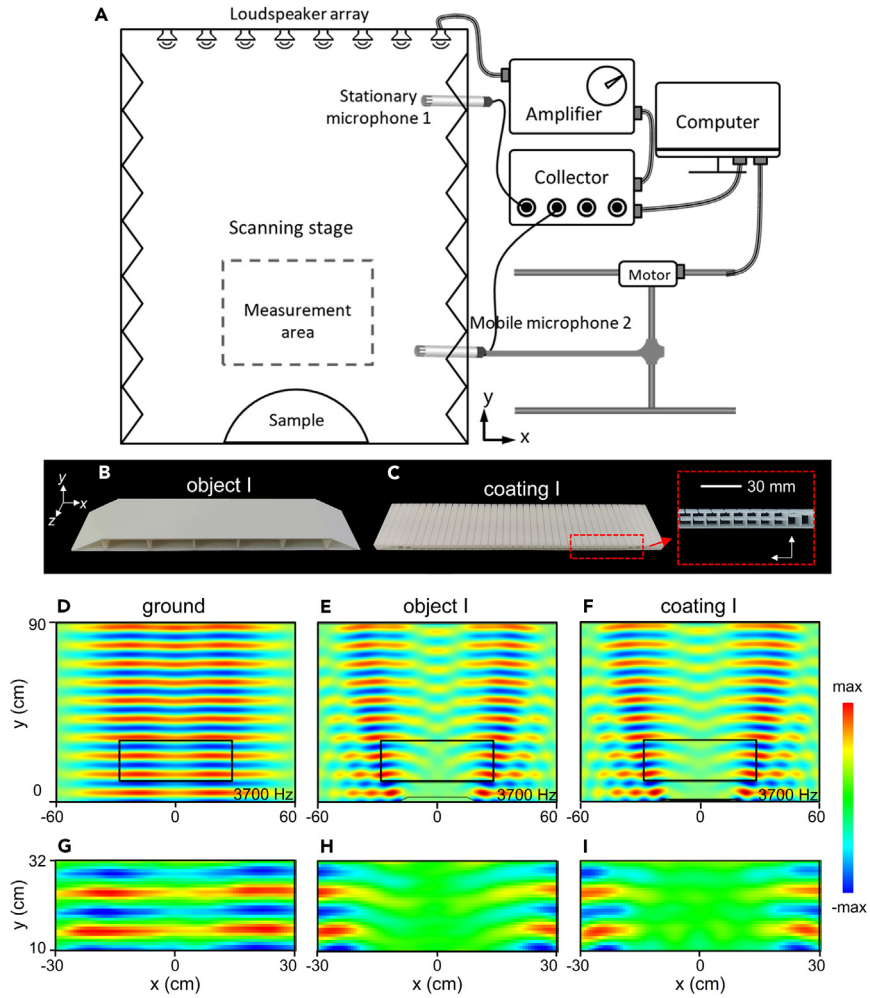

Figure 3. Experimental configuration and 2D acoustic illusion of illusion coating I

(A) Schematic of the experimental 2D acoustic pressure field scanning platform.

(B and C) The photographs of trapezoidal object I and coating I. The insert illustrates the detail of the illusion coating.

(D–F) The simulated total fields of the flat ground, object I and coating I.

(G–I) The corresponding measured total fields of the flat ground, object I and coating I. The black boxes in (D–F) indicate the measured areas in experiments.

experiments described here, the samples of illusion coatings are fabricated via a 3D printer whose manufacturing precision is 0.02 mm. The printed material is resin. To perform the measurement in laboratory, we build a 2D waveguide (120 × 200 cm^2 of the profile) composed of two paralleled plexiglass plates, as shown in Figure 3A. The density of the plates is 1200 $kg \cdot m^{-3}$, which is much larger than the density of air. Hence the plates are rigid enough to be regard as hard boundaries. The total fields are monitored and recorded by a scanning stage with two phase-matched 1/4-inch microphones (one is fixed for reference and another is moveable for signal detection). Eight identical loudspeakers (2 inches in diameter) are arranged on the top of the waveguide for generating a plane wave. In order to minimize the echo and environmental noise, absorbing sponges are installed around the waveguide closely. The distance between the upper and lower surfaces is 8 cm, which is set as the height of the sample. Therefore, the cut-off frequency of the 1st order mode of the waveguide is 2145 Hz. As a result, for our studied frequency 3700 Hz, there are higher order mode waves transmitting in the waveguide and the experiments could be regarded as full-wave works approximately.

Illusion coating I is designed for achieving a total field the same as a trapezoidal object I (Figure S1) out of thin air. The samples of object I and coating I are shown in Figures 3B and 3C. The insert shows the detail of the metacells of the illusion coating. Assuming that a plane acoustic wave travels along -*y* direction straightly on a flat ground, the wavefront of acoustic wave will be planar as well, as shown in Figure 3D. On the surface of the flat ground, there is no phase mutation between the scattered wave and the incident wave. When we place an illusion coating on the flat ground, whose phase gradient distribution of the scattered wave is designed the same as object I, the total acoustic field will be modulated accordingly, as shown in Figure 3F. It seems that a "trapezoid" is on the ground in spite of the fact that nothing else but an illusion coating is there. The coating is realized by the metasurface cells whose modulation of phase is delicately calculated (Table S1). The

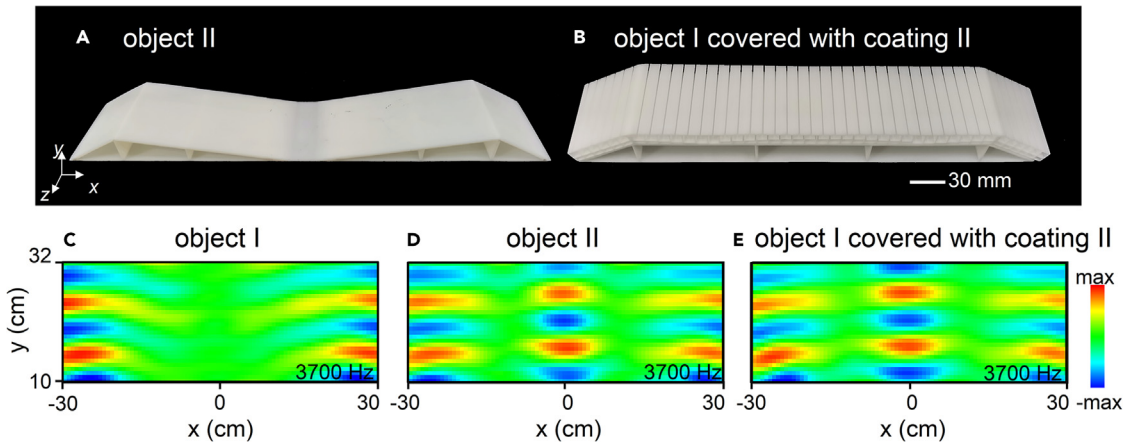

Figure 4. 2D acoustic illusion of illusion coating II

(A and B) The photograph of object II and that of object I covered with conformal coating II. The bottom row shows the measured total field of (C) object I, (D) object II and (E) object I covered with coating II.

total field of the trapezoid object I is achieved in numerical simulation for comparison, as shown in Figure 3E. These acoustic fields indicate that illusion coatings can create illusions that mimic the scattering fields of desired objects effectively.

In order to further verify the illusion performance of the illusion coating, we also measure the total fields experimentally. Figure 3I shows the measured total field of coating I that installed on the ground. It illustrates that an illusion with trapezoid-shape appears in air by inducing the illusion coating instead of a real trapezoid (object I). For comparison, the total fields of the flat ground and object I are measured as well, as shown in Figures 3G and 3H. The total field of object I is in accordance with the illusion perfectly. It suggests that the total fields generated by the illusion coating and object I are quite similar that the detector is cheated and disable to recognize the difference. It is a strong certification that the designed illusion coating could flexibly create an illusion out of thin air.

Then we perform another work to show that the designed illusion coating is capable to mimic the scattering field of desired object by attaching metacells on the surface of the detected target. Coating II is designed for cutting object I into two small triangles (object II) to the observers. The fabricated samples of object II and coating II are shown in Figures 4A and 4B. As shown in Figure 4E, experiments are performed to illustrate the total field of object I covered with an illusion coating II (Table S2). The total field caused by the two triangles is also measured for comparison in Figure 4D, which is similar to Figure 4E under the 2D scanning stage. For convenient for comparing, the color pattern Figure 3H is repainted in Figure 4C. It certifies that the illusion coating is capable to change the acoustic field of an object under the total cover to another profile by delicately calculating.

In addition, Figure 5 shows another interesting application of the illusion coating for objects with two triangles and an enlarged trapezoid. In order to further study the performance of the illusion coating without totally covered structures, we design an enlarged trapezoidal object III which is partially same as object II, as shown in Figure 5A. With delicately calculation, we choose the appropriate metacells to fabricate coating III (Table S3) for changing object II to the object III. The photograph of the illusion coating is shown in Figure 5B. The measured results (Figures 5C–5E) show that the total field of object II partially covered with coating III is similar to the total field of object III. It means that the object can also avoid being detected effectively under the partial cover of the illusion coating.

DISCUSSION

As illustrated in all these simulations and experiments, the illusion coatings designed by the metacells can modulate the scattering performance of the objects flexibly. It indicates that the illusion coatings provide a new platform to interfere with military detection.

Because the metacells working away from the resonant frequency shown in Figure 2B, the phase shifts change conformably at different frequencies with the varying structural parameter *d*. This characteristic makes the designed metacells advantageous to fabricate broadband metasurface for controlling the scatterings of acoustic waves. Therefore, we study the working frequency range of the illusion coating II that transfers the scattering fields of the object I to object II. As shown in Figure 6, numerical simulations are performed to illustrate the total fields of object I covered with the illusion coating II. In this work, the working frequency for designing coating II is 3700 Hz. It is exciting to find that the effective frequency range of the illusion coating is from 3000 Hz (Figures 6A and 6B) to 4500 Hz (Figures 6E and 6F). The corresponding measured results of particular frequencies 3000 Hz (Figures 6C and 6D) and 4500 Hz (Figures 6G and 6H) are also performed. It certifies that the illusion coating is capable to mimic the scattering field of desired object by delicate calculation in a broadband with a bandwidth 40.5%.

Limitations of the study

In summary, we have proposed broadband conformal acoustic illusion coatings for creating an illusion or mimicking the scattering field of desired object under the total or partial cover. The broadband illusion performances of the illusion coatings are demonstrated in simulations

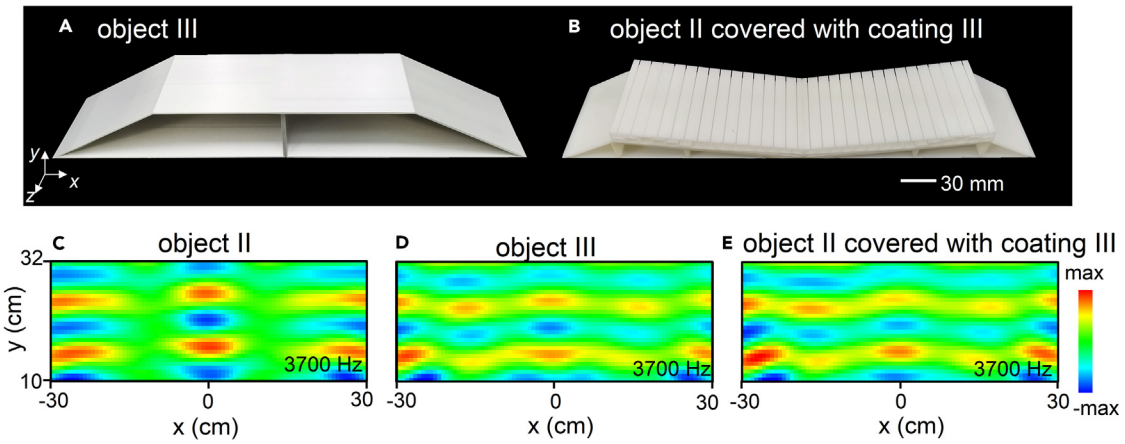

Figure 5. 2D acoustic illusion of illusion coating III

(A and B) The photograph of object III and that of object II covered with conformal coating III. The bottom row shows the measured total field of (C) object II, (D) object III and (E) object II covered with coating III.

and verified in experiments. In addition, the ultrathin illusion coatings are conformal with the detected targets, minimizing the additional bulk of the acoustic device. In this study, the bandwidth of acoustic illusion coatings has been effectively broadened compared to other acoustic illusion work. However, it is still limited to a specific frequency range. Furthermore, acoustic illusion coatings are more effective in vertical incident sound waves and are limited in oblique incident sound waves. Therefore, realizing impedance matching between the metasurface and air acoustic wave in the case of large-angle incidence is an urgent issue that requires attention. In addition, our discussion is limited to air media and does not consider the field of underwater acoustics, which requires intensive and extensive research to elucidate the general principles.

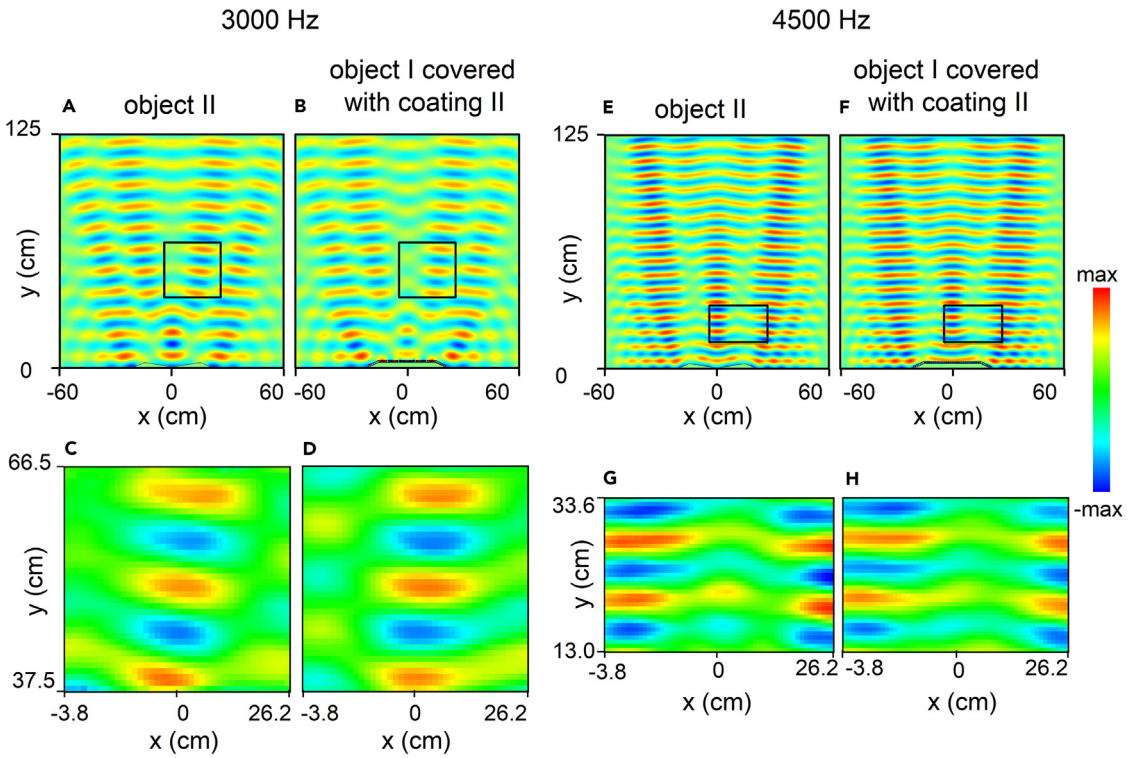

Figure 6. Simulated and measured 2D acoustic illusion of broadband illusion coating II

The total fields of object II and object I covered with coating II at the particular frequencies (A–D) 3000 Hz and (E–H) 4500 Hz. The top row shows the simulated results and the bottom row shows the corresponding measured results. The black boxes indicate the measured areas in experiments.

STAR★METHODS

Detailed methods are provided in the online version of this paper and include the following:

- KEY RESOURCES TABLE
- RESOURCE AVAILABILITY
  - Lead contact
  - Materials availability
  - Data and code availability
- EXPERIMENTAL MODEL AND STUDY PARTICIPANT DETAILS
- METHOD DETAILS
- QUANTITATION AND STATISTICAL ANALYSIS
- ADDITIONAL RESOURCES

SUPPLEMENTAL INFORMATION

Supplemental information can be found online at https://doi.org/10.1016/j.isci.2024.110504.

ACKNOWLEDGMENTS

The authors acknowledge the financial support from the National Key R&D Program of China (grant no. 2022YFB3806000, 2023YFB3811400), the National Natural Science Foundation of China (grant no. 12074314, 61771402), the Science and Technology New Star Program of Shaanxi Province (grant no. 2023KJXX-148), and the Fundamental Research Funds for the Central Universities.

AUTHOR CONTRIBUTIONS

K.S.: conceptualization, methodology, software, formal analysis, investigation, data curation, writing – original draft, writing – review & editing. F.Z.: resources, writing – review & editing, supervision, funding acquisition. S.C.: methodology, software, investigation, writing – original draft. Q.F.: validation, writing – review & editing, project administration. Y.Z.: writing – review & editing, supervision, Y.F.: validation, writing – review & editing, supervision, funding acquisition.

DECLARATION OF INTERESTS

The authors declare no competing interests.

Received: April 5, 2024
Revised: July 1, 2024
Accepted: July 11, 2024
Published: July 14, 2024

REFERENCES

1. Liu, Z., Zhang, X., Mao, Y., Zhu, Y.Y., Yang, Z., Chan, C.T., and Sheng, P. (2000). Locally resonant sonic materials. Science *289*, 1734–1736. https://doi.org/10.1126/science.289.5485.1734.
2. Fang, N., Xi, D., Xu, J., Ambati, M., Srituravanich, W., Sun, C., and Zhang, X. (2006). Ultrasonic metamaterials with negative modulus. Nat. Mater. *5*, 452–456. https://doi.org/10.1038/nmat1644.
3. Yang, Z., Mei, J., Yang, M., Chan, N.H., and Sheng, P. (2008). Membrane-type acoustic metamaterial with negative dynamic mass. Phys. Rev. Lett. *101*, 204301. https://doi.org/10.1103/PhysRevLett.101.204301.
4. Li, J., and Chan, C.T. (2004). Double-negative acoustic metamaterial. Phys. Rev. E *70*, 055602. https://doi.org/10.1103/PhysRevE.70.055602.
5. Zhang, X., Davanço, M., Urzhumov, Y., Shvets, G., and Forrest, S.R. (2008). From scattering parameters to snell's law: a subwavelength near-infrared negative-index metamaterial. Phys. Rev. Lett. *101*, 267401. https://doi.org/10.1103/PhysRevLett.101.267401.
6. Lee, S.H., Park, C.M., Seo, Y.M., Wang, Z.G., and Kim, C.K. (2010). Composite acoustic medium with simultaneously negative density and modulus. Phys. Rev. Lett. *104*, 054301. https://doi.org/10.1103/PhysRevLett.104.054301.
7. Chen, S., Fan, Y., Fu, Q., Wu, H., Jin, Y., Zheng, J., and Zhang, F. (2018). A review of tunable acoustic metamaterials. Appl. Sci. *8*, 1480. https://doi.org/10.3390/app8091480.
8. Zhu, Y., Hu, J., Fan, X., Yang, J., Liang, B., Zhu, X., and Cheng, J. (2018). Fine manipulation of sound via lossy metamaterials with independent and arbitrary reflection amplitude and phase. Nat. Commun. *9*, 1632. https://doi.org/10.1038/s41467-018-04103-0.
9. Shen, C., Xu, J., Fang, N.X., and Jing, Y. (2014). Anisotropic complementary acoustic metamaterial for canceling out aberrating layers. Phys. Rev. X *4*, 041033. https://doi.org/10.1103/PhysRevX.4.041033.
10. Liu, T., Zhu, X., Chen, F., Liang, S., and Zhu, J. (2018). Unidirectional wave vector manipulation in two-dimensional space with an all passive acoustic parity-time-symmetric metamaterials crystal. Phys. Rev. Lett. *120*, 124502. https://doi.org/10.1103/PhysRevLett.120.124502.
11. Fu, Y., Shen, C., Cao, Y., Gao, L., Chen, H., Chan, C.T., Cummer, S.A., and Xu, Y. (2019). Reversal of transmission and reflection based on acoustic metagratings with integer parity design. Nat. Commun. *10*, 2326. https://doi.org/10.1038/s41467-019-10377-9.
12. Gao, H., Fang, X., Gu, Z., Liu, T., Liang, S., Li, Y., and Zhu, J. (2019). Conformally mapped multifunctional acoustic metamaterial lens for spectral sound guiding and talbot effect. Research *2019*, 1748537. https://doi.org/10.34133/2019/1748537.
13. Tang, Y., Zhang, Y., Xie, B., Cheng, H., Tian, J., and Chen, S. (2022). Transmission-reflection-integrated multifunctional continuously tunable metasurfaces for decoupled modulation of acoustic Waves. Phys. Rev. Appl. *17*, 044027. https://doi.org/10.1103/PhysRevApplied.17.044027.
14. Zhang, S., Xia, C., and Fang, N. (2011). Broadband acoustic cloak for ultrasound waves. Phys. Rev. Lett. *106*, 024301. https://doi.org/10.1103/PhysRevLett.106.024301.

15. Hu, C., Yin, Y., and Chen, H. (2022). Three-dimensional omnidirectional acoustic illusion. Phys. Rev. Appl. *18*, 024049. https://doi.org/10.1103/PhysRevApplied.18.024049.
16. Chen, H., and Chan, C.T. (2007). Acoustic cloaking in three dimensions using acoustic metamaterials. Appl. Phys. Lett. *91*, 183518. https://doi.org/10.1063/1.2803315.
17. Xie, B., Tang, K., Cheng, H., Liu, Z., Chen, S., and Tian, J. (2017). Coding acoustic metasurfaces. Adv. Mater. *29*, 1603507. https://doi.org/10.1002/adma.201603507.
18. Xie, Y., Wang, W., Chen, H., Konneker, A., Popa, B.-I., and Cummer, S.A. (2014). Wavefront modulation and subwavelength diffractive acoustics with an acoustic metasurface. Nat. Commun. *5*, 5553. https://doi.org/10.1038/ncomms6553.
19. Assouar, B., Liang, B., Wu, Y., Li, Y., Cheng, J.-C., and Jing, Y. (2018). Acoustic metasurfaces. Nat. Rev. Mater. *3*, 460–472. https://doi.org/10.1038/s41578-018-0061-4.
20. Tian, Z., Shen, C., Li, J., Reit, E., Gu, Y., Fu, H., Cummer, S.A., and Huang, T.J. (2019). Programmable acoustic metasurfaces. Adv. Funct. Mater. *29*, 1808489. https://doi.org/10.1002/adfm.201808489.
21. Shen, C., Díaz-Rubio, A., Li, J., and Cummer, S.A. (2018). A surface impedance-based three-channel acoustic metasurface retroreflector. Appl. Phys. Lett. *112*, 183503. https://doi.org/10.1063/1.5025481.
22. Fan, S.-W., Zhao, S.-D., Chen, A.L., Wang, Y.-F., Assouar, B., and Wang, Y.-S. (2019). Tunable broadband reflective acoustic metasurface. Phys. Rev. Appl. *11*, 044038. https://doi.org/10.1103/PhysRevApplied.11.044038.
23. Liao, Y., Zhou, X., Chen, Y., and Huang, G. (2018). Adaptive metamaterials for broadband sound absorption at low frequencies. Smart Mater. Struct. *28*, 025005. https://doi.org/10.1088/1361-665x/aaeceb.
24. Chen, S., Fan, Y., Yang, F., Jin, Y., Fu, Q., Zheng, J., and Zhang, F. (2019). Engineering coiling-up space metasurfaces for broadband low-frequency acoustic absorption. Phys. Status Solidi RRL *13*, 1900426. https://doi.org/10.1002/pssr.201900426.
25. Zhu, Y., Fan, X., Liang, B., Cheng, J., and Jing, Y. (2017). Ultrathin acoustic metasurface-based schroeder diffuser. Phys. Rev. X *7*, 021034. https://doi.org/10.1103/PhysRevX.7.021034.
26. Ma, G., Yang, M., Xiao, S., Yang, Z., and Sheng, P. (2014). Acoustic metasurface with hybrid resonances. Nat. Mater. *13*, 873–878. https://doi.org/10.1038/nmat3994.
27. Li, H.-X., Rosendo-López, M., Zhu, Y.-F., Fan, X.-D., Torrent, D., Liang, B., Cheng, J.-C., and Christensen, J. (2019). Ultrathin acoustic parity-time symmetric metasurface cloak. Research *2019*, 8345683. https://doi.org/10.34133/2019/8345683.
28. Sun, K., Fan, Y., Chen, S., Yang, F., Li, J., Fu, Q., and Zhang, F. (2022). Highly efficient transmissive wavefront steering with acoustic metagrating composed of Helmholtz-resonators. Mater. Des. *224*, 111352. https://doi.org/10.1016/j.matdes.2022.111352.
29. Bai, Y., Song, A., Sun, C., Xiang, Y., and Xuan, F.-Z. (2023). Broadband sound focusing with tunable focus based on reconfigurable acoustic coding metagrating. Appl. Phys. Lett. *122*, 261705. https://doi.org/10.1063/5.0152748.
30. Xu, M., Harley, W.S., Ma, Z., Lee, P.V.S., and Collins, D.J. (2023). Sound-Speed modifying acoustic metasurfaces for acoustic holography. Adv. Mater. *35*, 2208002. https://doi.org/10.1002/adma.202208002.
31. Liu, C., Ye, Y., and Wu, J.H. (2023). Tunable broadband acoustic vortex generator with multiple orders based on Mie resonances structure. Adv. Mater. Technol. *8*, 2202082. https://doi.org/10.1002/admt.202202082.
32. Li, Y., and Assouar, B.M. (2016). Acoustic metasurface-based perfect absorber with deep subwavelength thickness. Appl. Phys. Lett. *108*, 063502. https://doi.org/10.1063/1.4941338.
33. Zigoneanu, L., Popa, B.-I., and Cummer, S.A. (2011). Design and measurements of a broadband two-dimensional acoustic lens. Phys. Rev. B *84*, 024305. https://doi.org/10.1103/PhysRevB.84.024305.
34. Chen, J., Xiao, J., Lisevych, D., Shakouri, A., and Fan, Z. (2018). Deep-subwavelength control of acoustic waves in an ultra-compact metasurface lens. Nat. Commun. *9*, 4920. https://doi.org/10.1038/s41467-018-07315-6.
35. Jiang, X., Li, Y., Liang, B., Cheng, J.-C., and Zhang, L. (2016). Convert acoustic resonances to orbital angular momentum. Phys. Rev. Lett. *117*, 034301. https://doi.org/10.1103/PhysRevLett.117.034301.
36. Yang, Y., Wang, H., Yu, F., Xu, Z., and Chen, H. (2016). A metasurface carpet cloak for electromagnetic, acoustic and water waves. Sci. Rep. *6*, 20219. https://doi.org/10.1038/srep20219.
37. Jin, Y., Fang, X., Li, Y., and Torrent, D. (2019). Engineered diffraction gratings for acoustic cloaking. Phys. Rev. Appl. *11*, 011004. https://doi.org/10.1103/PhysRevApplied.11.011004.
38. Esfahlani, H., Karkar, S., Lissek, H., and Mosig, J.R. (2016). Acoustic carpet cloak based on an ultrathin metasurface. Phys. Rev. B *94*, 014302. https://doi.org/10.1103/PhysRevB.94.014302.
39. Li, Y., Ren, Z., Yuan, X., Chen, M., Cao, W., Cheng, Q., Jin, Z., Cheng, X., Zhang, C., Yang, J., and Fang, D. (2019). Reflection phase dispersion editing generates wideband invisible acoustic Huygens's metasurface. J. Acoust. Soc. Am. *146*, 166–171. https://doi.org/10.1121/1.5116012.
40. Wang, Y., Cheng, Y., and Liu, X. (2019). Ultrathin acoustic cloaking by a conformal hybrid metasurface. Sci. Rep. *9*, 12700. https://doi.org/10.1038/s41598-019-49148-3.
41. Lai, Y., Ng, J., Chen, H., Han, D., Xiao, J., Zhang, Z.-Q., and Chan, C.T. (2009). Illusion optics: The optical transformation of an object into another object. Phys. Rev. Lett. *102*, 253902. https://doi.org/10.1103/PhysRevLett.102.253902.
42. Sun, F., Zhang, Y.J., Evans, J., and He, S.L. (2019). A camouflage device without metamaterials. Prog. Electromag. Res. *165*, 107–117. https://doi.org/10.2528/PIER19080803.
43. Jia, Y., Qian, C., Fan, Z., Ding, Y., Wang, Z., Wang, D., Li, E.-P., Zheng, B., Cai, T., and Chen, H. (2022). In situ customized illusion enabled by global metasurface reconstruction. Adv. Funct. Mater. *32*, 2109331. https://doi.org/10.1002/adfm.202109331.
44. Wang, R., Wang, B.Z., Gong, Z.S., and Ding, X. (2017). Creation of an arbitrary electromagnetic illusion using a planar ultrathin metasurface. IEEE Photonics J. *9*, 1–9. https://doi.org/10.1109/JPHOT.2017.2733044.
45. Liu, Y., Liang, Z., Liu, F., Diba, O., Lamb, A., and Li, J. (2017). Source illusion devices for flexural lamb waves using elastic metasurfaces. Phys. Rev. Lett. *119*, 034301. https://doi.org/10.1103/PhysRevLett.119.034301.
46. Zeng, Y., Zhou, Y., Zhou, M., and Chen, H. (2019). Illusion elastics in a fluid background. Phys. Rev. Appl. *11*, 014015. https://doi.org/10.1103/PhysRevApplied.11.014015.
47. Sun, F., Li, S., and He, S. (2017). Translational illusion of acoustic sources by transformation acoustics. J. Acoust. Soc. Am. *142*, 1213–1218. https://doi.org/10.1121/1.5000483.
48. Fan, S.-W., Zhao, S.-D., Cao, L., Zhu, Y., Chen, A.L., Wang, Y.-F., Donda, K., Wang, Y.-S., and Assouar, B. (2020). Reconfigurable curved metasurface for acoustic cloaking and illusion. Phys. Rev. B *101*, 024104. https://doi.org/10.1103/PhysRevB.101.024104.
49. Dubois, M., Shi, C., Wang, Y., and Zhang, X. (2017). A thin and conformal metasurface for illusion acoustics of rapidly changing profiles. Appl. Phys. Lett. *110*, 151902. https://doi.org/10.1063/1.4979978.
50. Chen, Z., Shao, S., Negahban, M., and Li, Z. (2019). Tunable metasurface for acoustic wave redirection, focusing and source illusion. J. Phys. D Appl. Phys. *52*, 395503. https://doi.org/10.1088/1361-6463/ab2abd.
51. Li, Y., Shen, C., Xie, Y., Li, J., Wang, W., Cummer, S.A., and Jing, Y. (2017). Tunable asymmetric transmission via lossy acoustic metasurfaces. Phys. Rev. Lett. *119*, 035501. https://doi.org/10.1103/PhysRevLett.119.035501.
52. Xie, B., Cheng, H., Tang, K., Liu, Z., Chen, S., and Tian, J. (2017). Multiband asymmetric transmission of airborne sound by coded metasurfaces. Phys. Rev. Appl. *7*, 024010. https://doi.org/10.1103/PhysRevApplied.7.024010.
53. Xia, J.-P., Zhang, X.-T., Sun, H.-X., Yuan, S.-Q., Qian, J., and Ge, Y. (2018). Broadband tunable acoustic asymmetric focusing lens from dual-Layer metasurfaces. Phys. Rev. Appl. *10*, 014016. https://doi.org/10.1103/PhysRevApplied.10.014016.
54. Shen, C., and Cummer, S.A. (2018). Harnessing multiple internal reflections to design highly absorptive acoustic metasurfaces. Phys. Rev. Appl. *9*, 054009. https://doi.org/10.1103/PhysRevApplied.9.054009.
55. Quan, L., and Alù, A. (2019). Passive acoustic metasurface with unitary reflection based on nonlocality. Phys. Rev. Appl. *11*, 054077. https://doi.org/10.1103/PhysRevApplied.11.054077.

STAR★METHODS

KEY RESOURCES TABLE

REAGENT or RESOURCE	SOURCE	IDENTIFIER
Software and algorithms		
COMSOL	COMSOL China Co., LTD	https://cn.comsol.com/

RESOURCE AVAILABILITY

Lead contact

Further information and requests for resources and reagents should be directed to and will be fulfilled by the lead contact, Fuli Zhang (fuli.zhang@nwpu.edu.cn).

Materials availability

This study did not generate new unique reagents.

Data and code availability

- Data reported in this paper will be shared by the lead contact upon request.
- This paper does not report original codes.
- Any additional information required to reanalyze the data reported in this paper is available from the lead contact upon request.

EXPERIMENTAL MODEL AND STUDY PARTICIPANT DETAILS

The COMSOL software has been employed to analyze the reflection curves, phases, and acoustic field distributions of the metasurface.

METHOD DETAILS

The simulations were based on COMSOL Multiphysics. The speed of acoustic waves and mass density of air are c_0 = 343 m/s and ρ_0 = 1.21 kg/m^3, respectively, and the amplitude of the incident plane wave is 1 Pa. The ultrathin metacells are set to sound rigid boundaries, and the background pressure field excites the incident plane waves.

QUANTITATION AND STATISTICAL ANALYSIS

The simulation data is produced by COMSOL Multiphysics software. The experimental data were tested in a self-built 2D waveguide acoustic test system. Figures shown in the main text were produced by ORIGIN and Microsoft PowerPoint from the raw data.

ADDITIONAL RESOURCES

Any additional information about the simulation and data reported in this paper is available from the lead contact on request.